TISSUE ENGINEERING: Part A
Volume 21, Numbers 15 and 16, 2015

DOI: 10.1089/ten.tea.2015.0089

termis
Tissue Engineering
& Regenerative Medicine
International Society

ORIGINAL ARTICLE

Modeling and Validation of Multilayer Poly(Lactide-Co-Glycolide) Scaffolds for *In Vitro* Directed Differentiation of Juxtaposed Cartilage and Bone

George X. Huang, BA,[1,2,*] Praveen R. Arany, BDS, MDS, MMSc, PhD,[1–4,*] and David J. Mooney, PhD[1,2]

Polymeric scaffolds, which release growth factors in a temporally controlled manner, have successfully directed the differentiation of stem cells into monolithic tissues of a single lineage. However, engineering precise boundaries in multilineage functional tissues, such as the juxtaposed cartilaginous and osseous tissue present in articulated joints, often remains a challenge. This work demonstrates a precise materials system for *in vitro* reconstruction of the three-dimensional architecture of these types of human tissues. Multilayer poly(lactide-co-glycolide) (PLG) scaffolds were used to produce spatiotemporal gradients to direct the differentiation of an initially uniform population of mesenchymal stem cells (MSCs) into juxtaposed cartilage and bone. Specifically, growth factors (chondrogenic transforming growth factor-β3 and osteogenic bone morphogenetic protein-4) and their neutralizing antibodies were incorporated within distinct layers of the PLG scaffolds to create spatially segregated morphogen fields within the scaffold volume. The multilayer PLG scaffold designs were optimized by mathematical modeling, and generation of spatially segregated morphogen gradients was validated by assessing activity of luciferase reporter cell lines responsive to each growth factor. Scaffolds seeded with MSCs demonstrated production of juxtaposed cartilage and bone, as evaluated by biochemical staining and western blotting for tissue-specific matrix proteins. This work demonstrates a significant advance for the engineering of implantable constructs comprising tissues of multiple lineages, with potential applications in orthopedic regenerative medicine.

Introduction

THERE EXISTS A GREAT medical need for the development of bioengineered implants, which can repair complex defects involving juxtaposed tissues of the body. For example, deterioration of juxtaposed cartilaginous and osseous tissue can occur due to osteoarthritis, osteochondritis dissecans, or traumatic injury.[1] Current treatment modalities for osteochondral defects include mechanical replacement of the joint tissue with prosthetic implants (typically comprising stainless steel, cobalt chrome, and polyethylene) or autologous grafting of millimeter-scale osteochondral plugs to the defect site (mosaicplasty). Artificial prostheses are susceptible to immune rejection, poor fit due to metal loosening, and the need for replacement due to long-term wear and tear.[2] Meanwhile, limitations of mosaicplasty include the lack of available donor tissue, donor site morbidity, and poor topological control of the grafts.[1–3] Over 400,000 joint replacement procedures are conducted in the United States every year[4] and demand is expected to rise significantly with increasing life expectancies.

In response to the shortage of tissues available for transplantation and the functional limitations of mechanical prostheses, tissue engineering often combines cultured cells with biocompatible three-dimensional (3D) scaffolds to assist the body's repair and regeneration processes. Using scaffold-based approaches to bioengineer juxtaposed cartilage and bone, offers the potential to overcome current deficiencies in treatment options for osteochondral disease. In embryonic development, dynamic gradients of bioactive signaling molecules carry positional information that specifies the fate of naïve stem-like cells into mature differentiated tissues. By using quantitative techniques to recapitulate morphogen gradients present during embryogenesis, tissue

[1]Harvard University School of Engineering and Applied Sciences, Cambridge, Massachusetts.
[2]Wyss Institute for Biologically Inspired Engineering, Harvard University, Cambridge, Massachusetts.
[3]Harvard School of Dental Medicine, Boston, Massachusetts.
[4]National Institutes of Dental and Craniofacial Research, National Institutes of Health, Bethesda, Maryland.
*These two authors contributed equally to this work.

engineers can potentially direct the differentiation of stem cells either seeded within or recruited to biocompatible scaffolds to generate functional organs of multiple tissue lineages.[5,6] Thus, these scaffolds not only provide an appropriate 3D environment that supports cell adhesion and survival but also can deliver biochemical cues, which influence cell differentiation and tissue maturation.[7,8]

We have recently proposed that one can engineer spatial boundaries in tissue formation with high spatial precision by mimicking development and releasing both promoters of tissue formation and their inhibitors from spatially distinct depots. This concept has been utilized to pattern the process of angiogenesis and to engineer juxtaposed dentin and bone, which has applications for dental reconstruction.[9,10] This study was based on the premise that multilayer poly(lactide-co-glycolide) (PLG) scaffolds could be utilized to produce temporally stable, spatially segregated morphogen gradients to direct the differentiation of juxtaposed hyaline cartilage and bone from an initially uniform population of naïve mesenchymal stem cells (MSCs). Transforming growth factor (TGF)-β3 was utilized as the chondrogenic cue,[11–14] while bone morphogenetic protein (BMP)-4 was utilized to promote osteogenesis.[15–17] Mathematical modeling was used to simulate morphogen concentration gradients and optimize the design of these complex scaffolds, and the generation of precisely controlled morphogen gradients was validated first using luciferase reporter cell lines, and then by analysis of the differentiation of MSCs seeded into the scaffolds.

Materials and Methods

Multilayer scaffold fabrication

Multilayer PLG scaffolds were fabricated from PLG microspheres as described previously[10] (Fig. 3A). Briefly, PLG microspheres (encapsulating desired proteins and/or small molecules) (see Supplementary Materials and Methods; Supplementary Data are available online at www.liebertpub.com/tea) were first mixed with NaCl particles that were sieved to a diameter between 250 and 425 μm at a mass ratio of 5% microspheres to 95% NaCl. The mixture was transferred into a custom steel mold (Fig. 3A, step 1), followed by light compaction with a hammer against the anvil to flatten the mixture (Fig. 3A, step 2). After each layer was added and compacted, the contents were compression molded into scaffold tablets at 2.5 MPa for 4 min in a hydraulic press (Carver) (Fig. 3A, step 3). Gas foaming and salt leaching were performed as described previously,[18,19] producing macroporous polymeric scaffolds containing interconnected pore structures. Briefly, compressed scaffold tablets were equilibrated with CO_2 at 800 psi for 16 h in a high-pressure vessel (Parr Instruments), followed by controlled rapid gas release to induce polymer foaming[19] (Fig. 3A, step 4). Salt was leached from the scaffold by immersion in distilled water, and scaffolds were dried by fluid wicking (Fig. 3A, step 5). Before use in cell culture, scaffolds were sterilized (70% ethanol for 10 min), washed twice with phosphate-buffered saline (10 min per wash), coated with serum proteins (100% fetal bovine serum [FBS] for 30 min), and again dried by fluid wicking.

To visualize the external distribution of layers, salt particles were mixed with orcein (Sigma-Aldrich) at a mass ratio of 1% dye to 99% NaCl for select layers. To visualize the internal distribution of layers, the radiocontrast agent, barium sulfate ($BaSO_4$; Sigma-Aldrich), was encapsulated in PLG microspheres used in select layers, and scaffolds were analyzed using a microcomputed tomography (micro-CT) instrument (X-Tek; Nikon Metrology) following salt leaching and desiccation.

Mathematical modeling

In 3D computational models, COMSOL Multiphysics (COMSOL) was used to simulate the concentration profiles of growth factors, antibodies, and growth factor–antibody complexes in multilayer scaffolds under *in vitro* culture conditions. These models accounted for release from scaffolds, diffusion, degradation, and binding kinetics. The governing partial differential equations of mass transport were as follows:

$$\frac{\partial GF}{\partial t} = D_{GF}\nabla^2(GF) + f_{GF}(t) - r_{GF}(GF) - k_{on,GF}(GF)(Ab) + k_{off,GF}(Complex)$$

$$\frac{\partial Ab}{\partial t} = D_{Ab}\nabla^2(Ab) + f_{Ab}(t) - r_{Ab}(Ab) - k_{on,Ab}(GF)(Ab) + k_{off,Ab}(Complex)$$

$$\frac{\partial (Complex)}{\partial t} = D_{Complex}\nabla^2(Complex) - r_{Complex}(Complex) + k_{on,Complex}(GF)(Ab) - k_{off,Complex}(Complex)$$

where GF denotes the concentration of free growth factor, Ab denotes the concentration of the free neutralizing antibody, $Complex$ denotes the concentration of growth factor–antibody complex, and D_i, $f_i(t)$, r_i, $k_{on,i}$, and $k_{off,i}$ denote the diffusivity, release function, uptake/degradation rate, binding rate, and dissociation rate of each species i, respectively.

The diffusivity of each species was calculated using the Young–Carroad–Bell method, $D_i = \frac{(8.34\times10^{-8})T}{\eta\left(M_i^{\frac{1}{3}}\right)}$, where T denotes the absolute temperature, η represents the dynamic viscosity of the fluid, and M represents the molecular weight of the protein.[20] Protein diffusion coefficients within the interior of the scaffolds were assumed to be 90% of those in still water, and perfect mixing was assumed in the liquid medium outside of the scaffolds. The protein release function (Equation 1 in Supplementary Data) was calculated by fitting the release profile of TGF-β1 from single-layer scaffolds (Supplementary Fig. S1A) to a third-order time-dependent polynomial. The uptake/degradation rates of TGF-β3 and BMP-4 were calculated by fitting the growth factor degradation profiles in the presence of MSCs (Supplementary Fig. S1B) to exponential decay functions and using the relationship, $r_i = \frac{\ln(2)}{t_{1/2}}$, where $t_{1/2}$ represents the fitted half-life of each species. The degradation rates of the antibodies and morphogen–antibody complexes were assumed to follow first-order kinetics with a half-life of 21 days.[21] The binding and dissociation rates were calculated using the relationship, $ND_{50} = \frac{k_{off}}{k_{on}}$, using the ND_{50} reported by the antibody manufacturer. The geometry of the liquid medium surrounding the scaffolds in the models reflected a 150-

mm-diameter Petri dish. A complete list of parameters used in the mathematical models can be found in Supplementary Table S2. The system geometry, governing equations, and initial conditions were constructed in COMSOL Multiphysics using the coefficient form, partial differential equation mode for time-dependent analysis, and the system of differential equations was solved using the generalized minimal residual method with incomplete lower-upper preconditioning.

MSC culture

For two-dimensional (2D) differentiation studies, murine D1 MSCs (ATCC) were plated in 24-well plates at a density of 30,000 cells/well in complete Dulbecco's Modified Essential Media (DMEM) with 10% FBS and 1× nonessential amino acids. After 24 h, media were replaced with Minimal Essential Media (αMEM) and various combinations of TGF-β3 (10 ng/mL), BMP-4 (15 ng/mL), neutralizing antibodies to TGF-β (1 μg/mL), and neutralizing antibodies to BMP-4 (1 μg/mL). These conditions were investigated in the presence of chondrogenic supplements (100 nM dexamethasone, 50 μg/mL ascorbic acid 2-phosphate, and 1× insulin–transferrin–selenium), osteogenic supplements (100 nM dexamethasone, 50 μg/mL ascorbic acid 2-phosphate, and 10 mM β-glycerophosphate), or both (100 nM dexamethasone, 50 μg/mL ascorbic acid 2-phosphate, insulin–transferrin–selenium, and 10 mM β-glycerophosphate). Media were replaced every 72 h.

For 3D culture, multilayer scaffolds were uniformly seeded with MSCs at 10×10^6 cells/scaffold. Scaffolds were then cultured in αMEM supplemented with 10% FBS, 1× nonessential amino acids, 100 nM dexamethasone, and 50 μg/mL ascorbic acid 2-phosphate under conditions of orbital shaking, with replacement of media every 7 days.

Luciferase activity assays

Mink lung epithelial cells (Mv1Lu) stably transfected with luciferase regulated by the plasminogen activator inhibitor promoter (PAI-Luc) and murine myoblasts (C2C12) stably transfected with luciferase regulated by BMP-responsive element promoter (BRE-Luc) were uniformly seeded onto scaffolds at a density of 10×10^6 cells/scaffold. After 24 h of culture in DMEM supplemented with 10% FBS, the scaffolds were immersed in coelenterazine and bioluminescence was recorded using the Xenogen IVIS-200 imaging system (Caliper). The luciferase activity exhibited by each zone of the scaffolds was then quantified using Living Image 3.2 (Caliper).

Western blotting

MSC cultures or scaffold specimens were sonicated (Sonics) and lysed in RIPA buffer (Sigma-Aldrich) containing Complete Mini protease inhibitor (Roche), and samples were normalized to total protein using the BCA assay (Pierce). Proteins were separated by sodium dodecyl sulfate–polyacrylamide gel electrophoresis in precast Tris-glycine gels (Invitrogen) and transferred onto nitrocellulose membranes using a semidry transfer process. Membranes were blocked with 3% bovine serum albumin (Sigma-Aldrich), incubated overnight at 4°C with primary antibody as per the manufacturer's instructions, and incubated with horseradish peroxidase-conjugated secondary antibodies (Jackson Immunoresearch) for 30 min at room temperature. Blots were incubated with the SuperSignal Chemiluminescent Substrate (Pierce) and developed using high-resolution radiographic films (Kodak).

Microcomputed tomography

After desiccation, scaffolds containing barium sulfate were analyzed using a micro-CT instrument (X-Tek; Nikon Metrology). A transmission source power of 90 kV, current of 90 μA, and 4-s exposure time were used. Frames were optimized based on the sample size ranging from 2900 to 3300 frames. A CCD panel detector (Perkin-Elmer) with 2000×2000 pixels, 7.5 fps, and pixel size of 200 μm was used to capture and reconstruct images with imaging software (InspectX and CT-Pro; Nikon Metrology).

Scanning electron microscopy and energy-dispersive X-ray spectroscopy

Scaffolds were fixed in cacodylate buffer containing 4% paraformaldehyde (Sigma-Aldrich) for 2 h and sectioned into 1-mm-thick slices. Fixed slices were bathed in 2% pyroantimonate (Electron Microscopy Sciences), an electron-dense agent that precipitates in the presence of calcium, for 1 h at RT. After desiccation, samples were sputter coated with platinum–palladium and analyzed by energy-dispersive X-ray spectroscopy (EDS) elemental analysis (Bruker Optics) in conjunction with backscatter scanning electron microscopy (SEM) imaging to detect crystalline deposits of antimonate.

Other biochemical assays

TGF-β1 enzyme-linked immunosorbent assay (ELISA; Promega) and BMP-4 ELISA (R&D Systems) were performed according to the manufacturer's instructions. Alizarin Red staining,[22] Alcian Blue staining,[23] alkaline phosphatase activity assay,[24] and Arsenazo III assay[25] were performed as previously described.

Statistical analysis

All values are reported as mean ± standard deviation, and biological replicates are denoted as. (n) The two-tailed Student's t-test was used to evaluate statistical significance, which was labeled with an asterisk (*) for p-values < 0.05.

Results

Selection of biochemical cues

Based on published reports, TGF-β3 and BMP-4 were chosen as morphogens to induce chondrogenic and osteogenic differentiation, respectively. We first evaluated the efficacy of these growth factors in the presence of supplements that enhance differentiation as well as in the presence of opposing neutralizing antibodies. TGF-β3 in chondrogenic media robustly induced expression of Sox9, a transcription factor marking chondrocyte differentiation, compared with untreated cells (negative control) after 48 h (Fig. 1A). This effect was preserved in the presence of the BMP-4-neutralizing antibody, indicating that the antibody does not cross-react with TGF-β3. However, the ability of TGF-β3 to induce Sox9 expression was unaffected by the addition of BMP-4 (only for the first 48 h). On the other

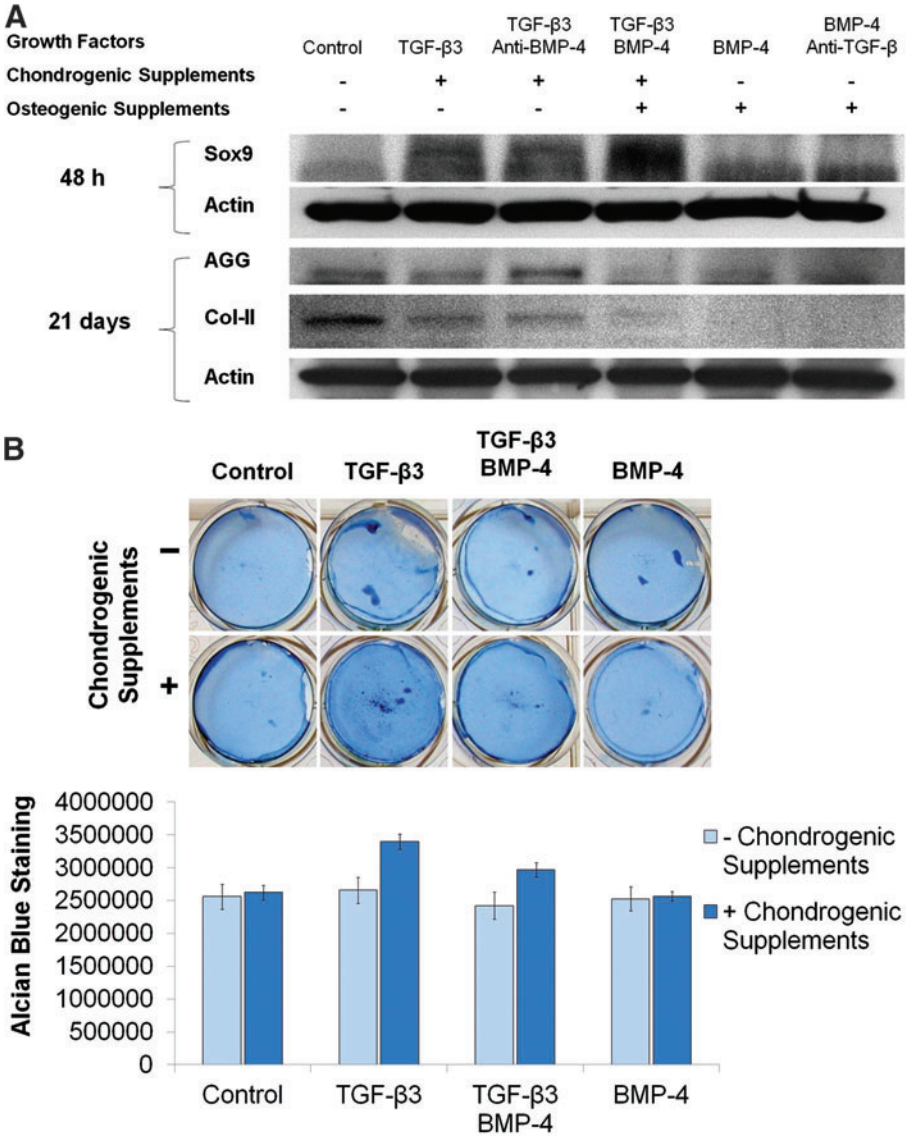

FIG. 1. Selection of chondrogenic cues. Mesenchymal stem cells (MSCs) were cultured in complete Minimal Essential Media (αMEM) with the indicated growth factors, antibodies, and supplements. **(A)** Cells were lysed and analyzed by western blotting for expression of Sox9 (48 h) and the cartilage matrix proteins, aggrecan (AGG) and type II collagen (Col-II) (21 days). β-Actin was used as loading control. **(B)** Cells were fixed after 14 days and stained with Alcian Blue. Representative photographs are shown in the *upper panel*, and quantification ($n=2$) is shown in the *lower panel*. Color images available online at www.liebertpub.com/tea

hand, treating MSCs with BMP-4 and osteogenic supplements (positive control) was found to inhibit production of cartilaginous extracellular matrix, namely aggrecan and type II collagen, compared with untreated cells after 21 days (Fig. 1A). This inhibition could not be rescued by the addition of TGF-β3 and chondrogenic supplements, underscoring the need for neutralization of BMP-4 in the chondrogenic zone of the scaffolds. MSCs treated with TGF-β3 required the addition of chondrogenic supplements to maximally upregulate the total glycosaminoglycan content, as indicated by the intensity of Alcian Blue staining after 14 days (Fig. 1B). This suggests that both TGF-β3 and chondrogenic supplements are required for mature chondrocyte differentiation in this system.

The effect of each factor on osteogenesis was next analyzed. We observed that the osteoblast transcription factor, Runx2, was expressed in untreated cells after 48 h of culture, suggesting a low-level basal differentiation of these cells to a bone-like phenotype (Fig. 2A). However, BMP-4 with osteogenic supplements further robustly induced calcium deposition as assessed by Arsenazo III assay and Alizarin Red staining compared with untreated cells after 14 days (Fig. 2B, C). In this study, the addition of TGF-β3 and chondrogenic supplements was noted to reduce calcium deposition in response to BMP-4 and osteogenic supplements, indicating the need for neutralization of TGF-β3 within an osteogenic zone of differentiation. The ability of BMP-4 to induce calcium deposition was slightly decreased by the addition of a neutralizing antibody to TGF-β. Furthermore, underscoring the requirement for controlling the spatial activity of these factors, the treatment with TGF-β3 and chondrogenic supplements was found to inhibit production of bone sialoprotein II and osteopontin compared with untreated cells after 21 days. This inhibition could not be rescued by the addition of BMP-4 and osteogenic supplements (Fig. 2A). While treatment with osteogenic supplements alone produced large increases in the intensity of Alizarin Red staining (Fig. 2C), both BMP-4 and osteogenic supplements were required for maximal induction of alkaline phosphatase activity after 14 days (Fig. 2D). This suggests that both BMP-4 and osteogenic supplements are required for mature osteoblast differentiation in this system.

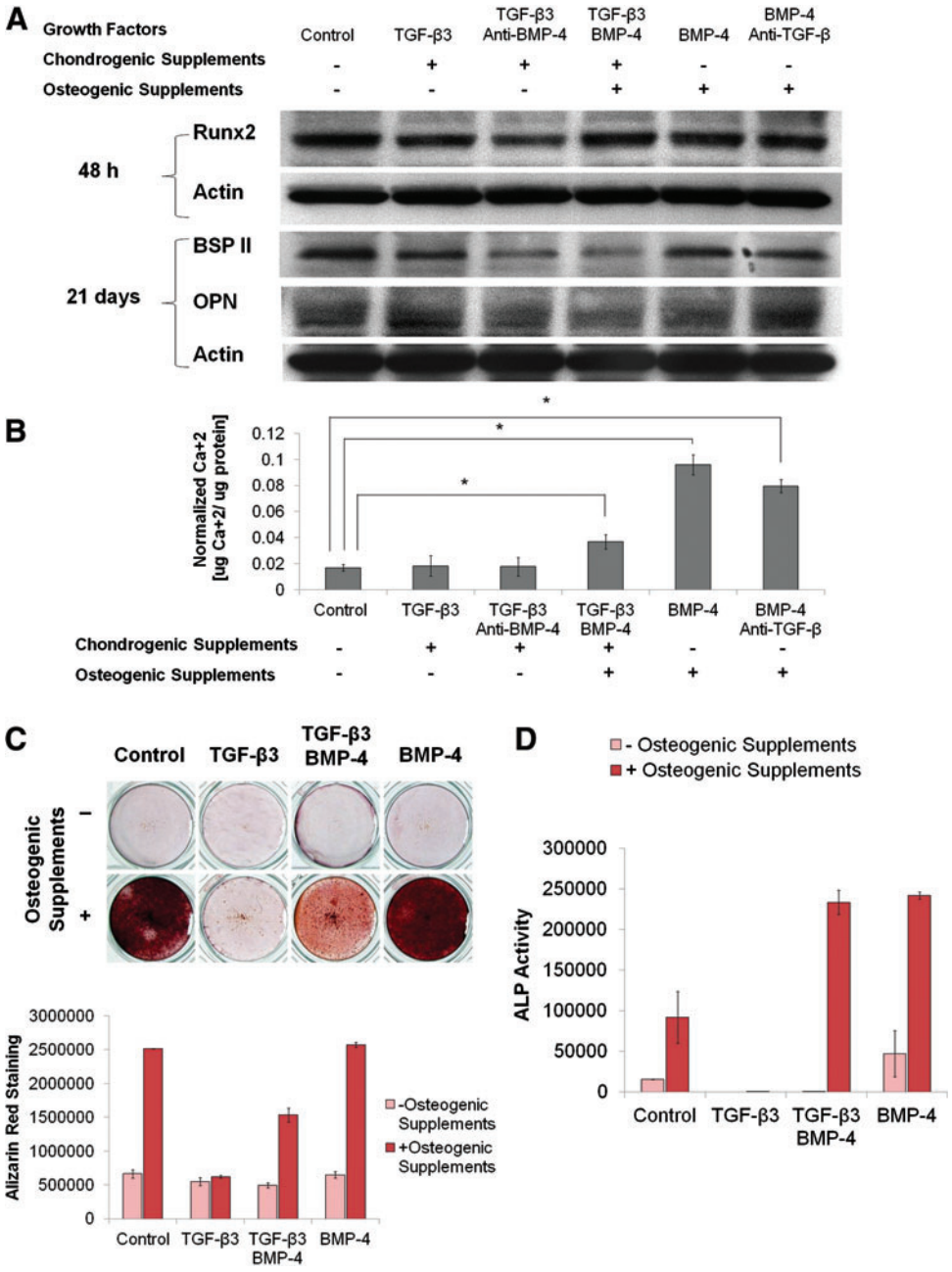

FIG. 2. Selection of osteogenic cues. MSCs were cultured in complete αMEM with the indicated growth factors, antibodies, and supplements. **(A)** Cells were lysed and analyzed by western blotting for expression of Runx2 (48 h) and for the bone matrix proteins, bone sialoprotein II (BSP II) and osteopontin (OPN) (21 days). β-Actin was used as loading control. **(B)** Cells were lysed after 14 days and analyzed with Arsenazo III assay for total calcium content ($n=4$). *Asterisks* indicate statistical significance at $p<0.05$. **(C)** Cells were fixed after 14 days and stained with Alizarin Red. Representative photographs are shown in the *upper panel*, and quantification ($n=2$) is shown in the *lower panel*. **(D)** Cells were lysed after 14 days and assayed for alkaline phosphatase (ALP) activity ($n=2$). Color images available online at www.liebertpub.com/tea

Based on these biochemical assays, TGF-β3 and insulin–transferrin–selenium were incorporated in the chondrogenic zones of the scaffolds, while BMP-4 and β-glycerophosphate were incorporated in the osteogenic zones of the scaffolds. The remaining supplements (dexamethasone and ascorbic acid) were supplemented in the culture medium, rather than incorporated in to the scaffold, as they are required throughout the entire scaffold volume.

Structural analysis of multilayered scaffolds

Multilayer PLG scaffolds were fabricated using a technique, in which the PLG microsphere–salt porogen mixture for each successive layer was lightly compacted by tapping a hammer against the cylindrical anvil, after which the entire scaffold was compressed into a tablet using the hydraulic press (Fig. 3A). This method of multilayer scaffold fabrication was evaluated for its ability to generate contiguous scaffolds with uniform layer thickness before using the multilayer scaffolds in cell culture studies. First, the spatial segregation of the distinct layers was visualized by incorporating the water-insoluble red dye, orcein, into the outer layers of three-layer scaffolds. Upon external inspection, the scaffolds exhibited layers of uniform thickness that were contiguous, with no distinct separations between layers (Fig. 3B). Second, to visualize segregation of layer contents throughout the scaffold interior, scaffolds were produced in which selected layers contained the insoluble contrast agent, barium sulfate. In this study, five-layer scaffolds, in which the second and fourth layers contained barium sulfate, were used because this allowed multiple nonadjacent layers within the scaffold interior to be

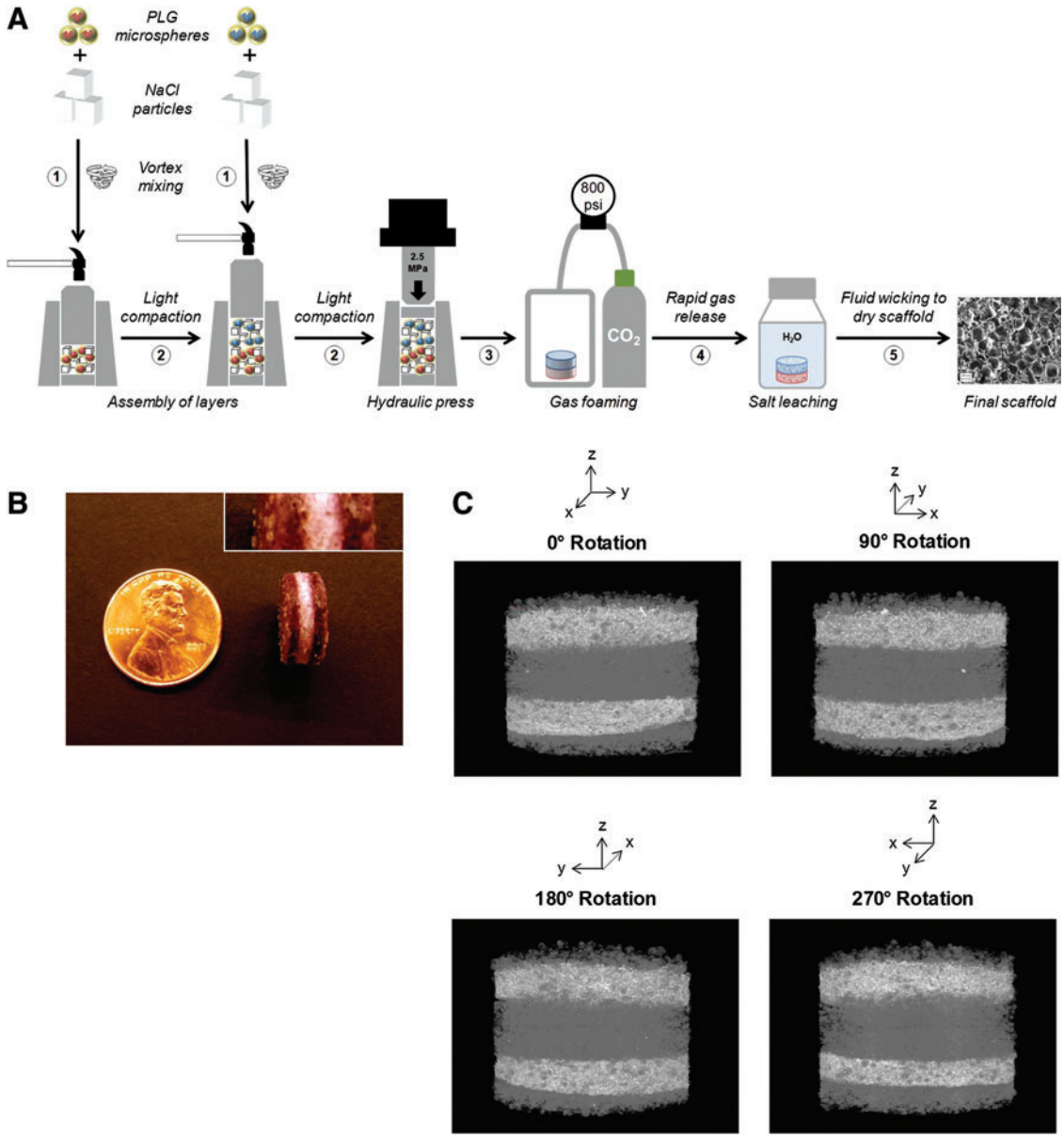

FIG. 3. Structural analysis of multilayer scaffolds. **(A)** Schematic illustration technique for fabrication of multilayer poly(lactide-co-glycolide) (PLG) scaffolds (details in the Materials and Methods section). Vortexed mixtures of PLG microspheres and sieved salt (NaCl) particles for each layer were sequentially added to the cylindrical scaffold mold (step 1) and lightly compacted with a hammer (step 2). The mold contents were then compressed in a hydraulic press at 2.5 MPa for 4 min to produce a scaffold tablet (step 3). The tablets were then equilibrated with 800 psi CO_2 for 16 h in a high-pressure chamber, followed by rapid gas release to induce foaming of the PLG polymer around salt particles (step 4). To generate a porous scaffold structure, salt was removed from the scaffold by immersing the foamed scaffolds in distilled water, and scaffolds were then dried by fluid wicking (step 5). Before cell seeding, scaffolds were sterilized by bathing in 70% ethanol for 10 min, washed twice with phosphate-buffered saline, and serum coated in 100% fetal bovine serum for 30 min. **(B)** Representative photograph of the external surface of a three-layer scaffold, in which outermost layers were highlighted using a red dye, orcein. *Inset* image (*top right*) shows higher magnification detail and a standard US penny for size comparison. **(C)** Perspectives at 90° rotations from microcomputed tomography reconstruction of a five-layer scaffold, in which $BaSO_4$ was incorporated in the second and fourth layers. Color images available online at www.liebertpub.com/tea

contrast labeled, permitting better analysis of layer uniformity. 3D reconstruction of micro-CT images of these scaffolds confirmed that each scaffold layer was macroscopically uniform in thickness, and no distinct separations were evident between any of the layers throughout the volume of the scaffold (Fig. 3C).

Scaffold design optimization and validation

Various multilayer scaffold designs were modeled and then fabricated to determine an appropriate design to yield spatially segregated gradients of TGF-β3 and BMP-4. Time-dependent mathematical modeling in COMSOL Multiphysics

was first used to optimize the dose of growth factors incorporated into each of the scaffold layers. Specifically, total concentrations of each species were adjusted until the mean concentration of TGF-β3 throughout the chondrogenic layer exceeded 0.10 ng/mL after 72 h and the mean concentration of BMP-4 throughout the osteogenic layer exceeded 0.15 ng/mL after 72 h. The 72-h time point was selected because it appropriately framed the burst phase of morphogen release from the scaffolds (Supplementary Fig. S1A), and concentration cutoffs were selected so that the mean morphogen concentration within the releasing layers did not drop below 1% of those used in the 2D differentiation studies at any point during the 72-h window.

Scaffolds were subsequently fabricated according to the optimized designs and seeded with luciferase reporter cells responsive to TGF-β (PAI-Luc) or BMP-4 (BRE-Luc). For assays using luciferase reporter cells, scaffolds were fabricated with TGF-β1 (a growth factor with similar molecular weight to TGF-β3) and assessed with the specific reporter cell line, p3TP-luciferase (PAI-Luc). The specificity (Supplementary Fig. S2) and dose responsiveness (Supplementary Fig. S3) of the PAI-Luc and BRE-Luc cell lines to TGF-β1 and BMP-4, respectively, were confirmed using single-layer scaffolds.

The first iteration of scaffold design was a three-layer scaffold system in which the outer layers were fabricated using microspheres, in which TGF-β3 or BMP-4 had been encapsulated, while the middle layer was fabricated from empty microspheres (Fig. 4A). COMSOL simulations of the optimized first-generation scaffolds demonstrated stable morphogen gradients that were maintained for several days. However, there seemed to be a significant overlap between zones of relatively high TGF-β3 and BMP-4 activity in the middle layer, and nontrivial concentrations of growth factors were predicted to diffuse across the length of the scaffold (Fig. 4B). Imaging of reporter cells seeded onto the scaffolds revealed that luciferase activity of PAI-Luc cells was maximal in zone A and luciferase activity of BRE-Luc cells was maximal in zone C; nonetheless, the scaffolds failed to produce statistically significant differences in integrated fluorescence density between zones A and C after 24 h (Fig. 4C). Thus, the multilayer scaffold design lacking neutralizing antibodies was deemed unsatisfactory for producing spatially segregated morphogen gradients.

In the second iteration of scaffold design, neutralizing antibodies to TGF-β3 and BMP-4 were incorporated in the middle layer between the layers containing TGF-β3 and BMP-4 in an effort to localize free morphogens to only their distinct zones of release. The thickness of the middle layer was doubled from the previous generation of scaffolds to minimize colocalization of morphogens. In addition, the diameter of the scaffolds was increased from 8 to 13 mm because larger scaffolds were easier to handle and dissect for analysis. To aid orientation of the cylindrical scaffolds, rhodamine-tagged nanoparticles were incorporated within a thin layer adjacent and external to the TGF-β3 layer as fiducial markers. To maintain symmetry of the scaffolds for analysis, another thin layer with no growth factors was added to the other side as well. The thickness of these outermost layers was designed to be 1.27 mm, the minimum size for which the mass of microspheres could be measured reliably (Supplementary Fig. S4A). COMSOL simulations of the optimized second-generation scaffolds predicted diminished migration of growth factors through the middle layer; however, it was observed that minute quantities of morphogens could diffuse beyond the middle layer into the opposing zones (Supplementary Fig. S4B). Imaging of reporter cells demonstrated that neutralizing antibodies effectively diminished bioactive growth factor levels in zone B of the scaffolds and statistically significant differences in luciferase activity were observed between zones A and C after 24 h (Supplementary Fig. S4C). However, several scaffolds seeded with PAI-Luc reporter cells exhibited greater fluorescence in zone C than zone B, and several scaffolds seeded with BRE-Luc reporter cells exhibited greater fluorescence in zone A than zone B, indicating that addition of antibodies to the middle layer alone was inadequate to neutralize opposing morphogens.

In the third iteration of scaffold design, neutralizing antibodies were added to all scaffold layers, except those releasing the specific morphogen (Fig. 5A). COMSOL simulations of the optimized third-generation scaffolds predicted successful segregation of morphogens in opposite regions of scaffolds (Fig. 5B). Luciferase imaging of reporter cells demonstrated statistically significant differences in luciferase activity between zones A and C, with no aberrant activity of non-neutralized morphogens in undesired locations after 24 h (Fig. 5C). Thus, the multilayer scaffold design with neutralizing antibodies throughout the opposing layers was successful in generating spatially distinct morphogen gradients.

Generation of juxtaposed cartilage and bone from MSCs

Scaffolds were produced according to the third-generation specifications (Fig. 6A), seeded uniformly with MSCs, and cultured *in vitro* for 21 days. Dual staining of scaffold cross sections with Alcian Blue and Alizarin Red resulted in intense Alcian Blue staining in zone A (indicative of glycosaminoglycan deposition consistent with cartilage formation), while distinct Alizarin Red staining was noted in zones B and C (indicative of calcium deposition consistent with bone formation) (Fig. 6B). SEM-EDS analysis following incubation of scaffolds with potassium pyroantimonate revealed the presence of electron-dense precipitates localized to zone C of the sections (Fig. 6C), indicating that mineralization was spatially restricted to the osteogenic zones. Scaffolds were also dissected and proteins collected for immunoblotting. Although lower amounts of protein were retrieved from zone B of the scaffolds, western blotting for matrix proteins revealed increased cartilage-specific matrix proteins (aggrecan and type II collagen) in zone A compared with zone C of the scaffolds, while bone-specific matrix proteins (bone sialoprotein II and osteopontin) were noted to be increased in zone C compared with opposing zones (Fig. 6D). These differences were statistically significant for aggrecan, type II collagen, and bone sialoprotein II ($p < 0.05$), but not for osteopontin ($p = 0.17$).

In addition, we probed each zone for expression of type X collagen, a marker of hypertrophic cartilage. Several of the scaffolds exhibited high levels of type X collagen in zone B (Fig. 6D), between the cartilaginous and osseous zones,

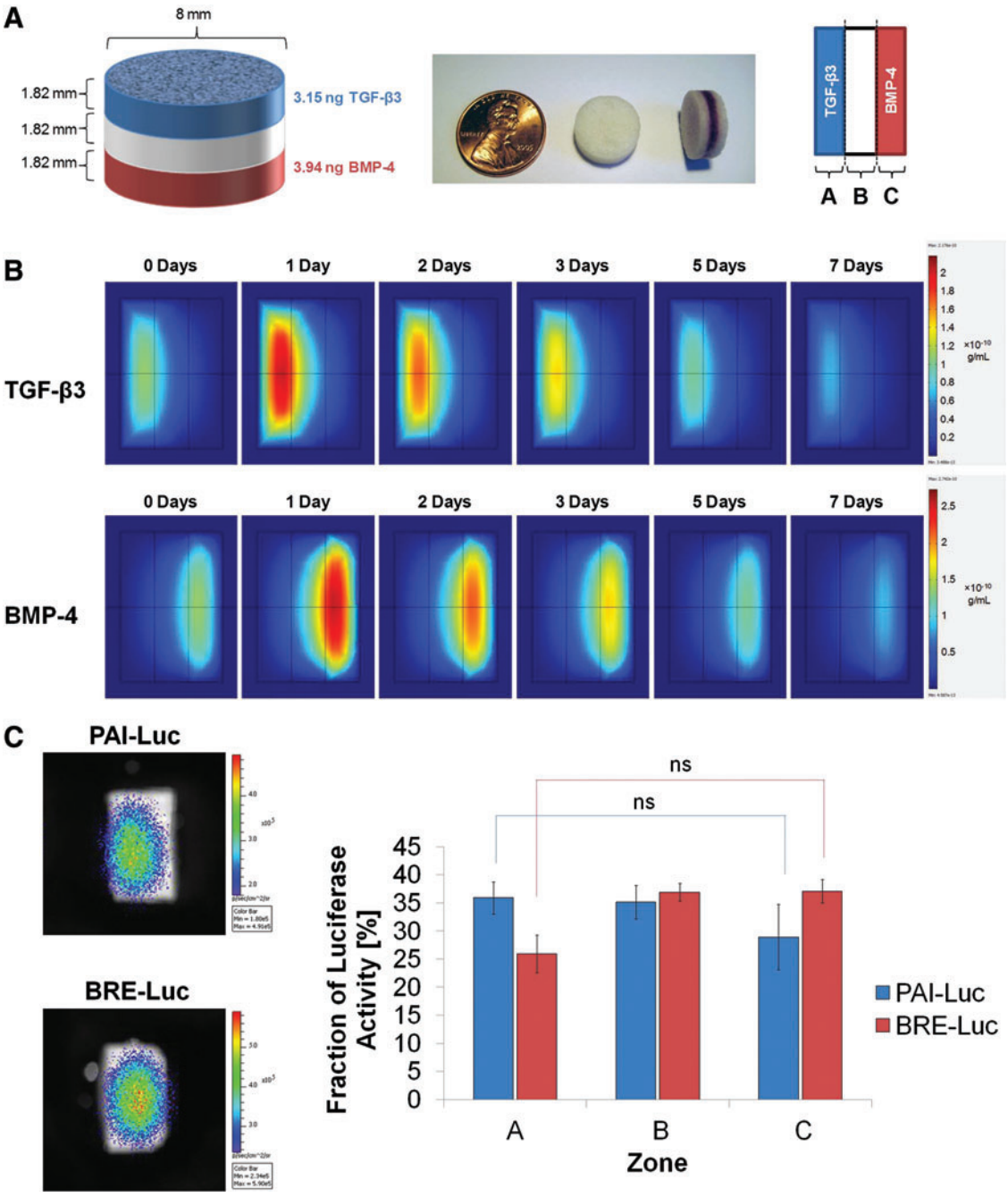

FIG. 4. Three-layer scaffold with no neutralizing antibodies (first-generation design). **(A)** Schematic of scaffold dimensions and contents after optimization by mathematical modeling (*left*); photographs of three-layer scaffolds, in which selected layers have been labeled with orcein (*middle*); and orientation of scaffolds for mathematical modeling and luciferase imaging (*right*). **(B)** Slice plots illustrating concentration profiles of transforming growth factor (TGF)-β3 (*upper row*) and bone morphogenetic protein (BMP)-4 (*lower row*) over 7 days, as simulated in COMSOL Multiphysics. Values reported in g/mL. **(C)** Representative images (*left*) and quantification (*right*) of photon flux density through scaffold zones at 24 h after seeding with PAI-Luc or BRE-Luc cells ($n = 3$ for each reporter line). Differences were not statistically significant ($p > 0.05$). Color images available online at www.liebertpub.com/tea

suggesting that the scaffold system recapitulated this aspect of endochondral ossification. Moreover, we also noted increased expression of type X collagen in zone A compared with zone C of the scaffolds. Altogether, these data suggest that spatially segregated morphogen gradients in multilayer scaffolds can promote differentiation of juxtaposed cartilage and bone for regenerative applications.

Discussion

In this study, we demonstrate materials that create spatially segregated gradients of TGF-β3 and BMP-4 to generate juxtaposed cartilage and bone. Specifically, mathematical modeling of concentration gradients for TGF-β3 and BMP-4 was used to optimize scaffold designs,

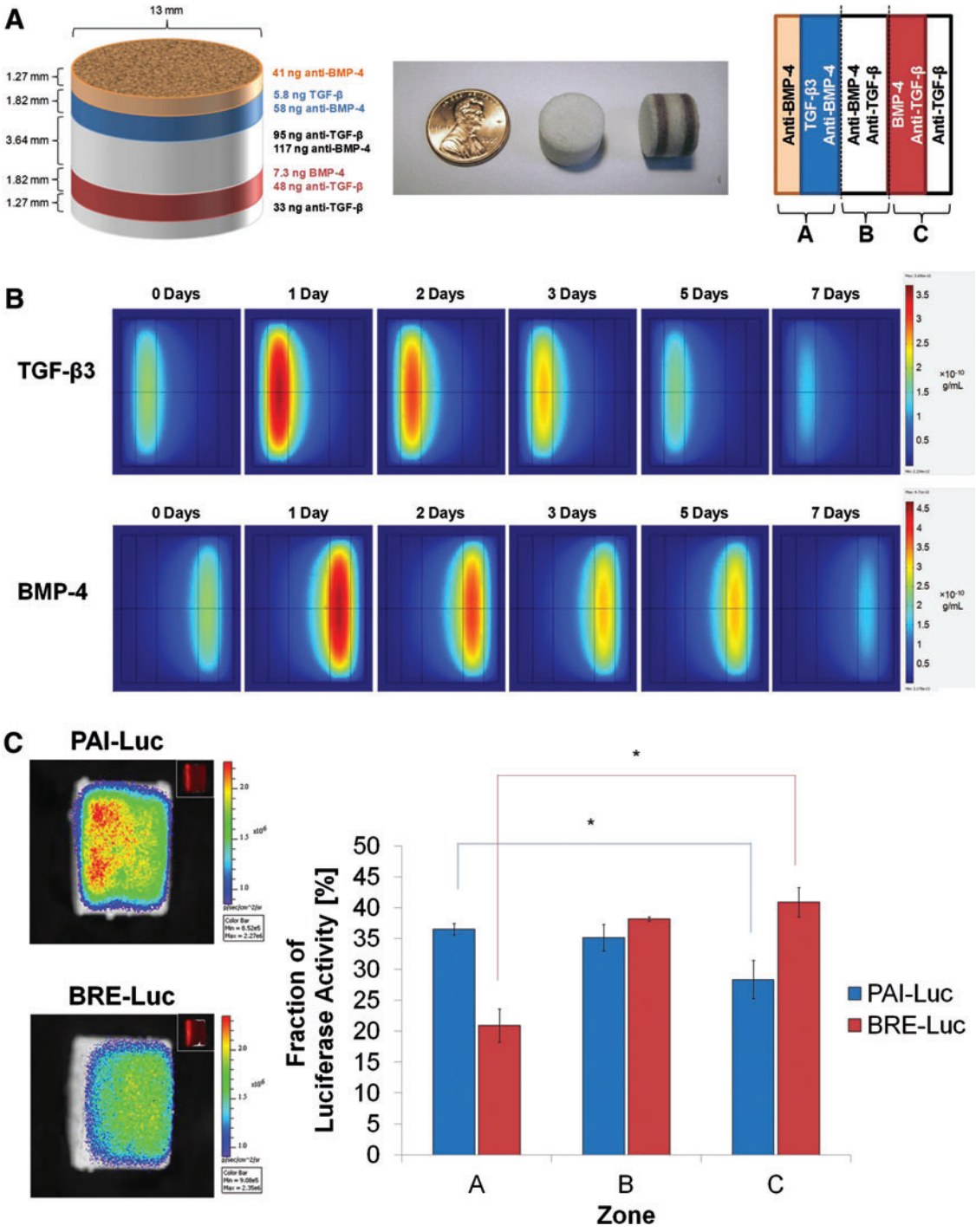

FIG. 5. Five-layer scaffold with neutralizing antibodies throughout (third-generation design). **(A)** Schematic of scaffold dimensions and contents after optimization by mathematical modeling (*left*); photographs of three-layer scaffolds, in which selected layers have been labeled with orcein (*middle*); and orientation of scaffolds for mathematical modeling and luciferase imaging (*right*). **(B)** Slice plots illustrating concentration profiles of TGF-β3 (*upper row*) and BMP-4 (*lower row*) over 7 days, as simulated in COMSOL Multiphysics. Values reported in g/mL. **(C)** Representative images (*left*) and quantification (*right*) of photon flux density through scaffold zones at 24 h after seeding with PAI-Luc or BRE-Luc cells ($n = 3$ for each reporter line). *Asterisks* indicate statistical significance at $p < 0.05$. Color images available online at www.liebertpub.com/tea

luciferase reporter cells were used to confirm the production of spatially segregated morphogen gradients, and analysis of extracellular matrix composition demonstrated successful preliminary formation of juxtaposed cartilage and bone.

Previously reported attempts to produce bioengineered osteochondral constructs have relied on differentiating MSCs into chondrogenic and osteogenic lineages before dissociating the cells and incorporating them into scaffolds.[2,4] Reliance on MSC differentiation before

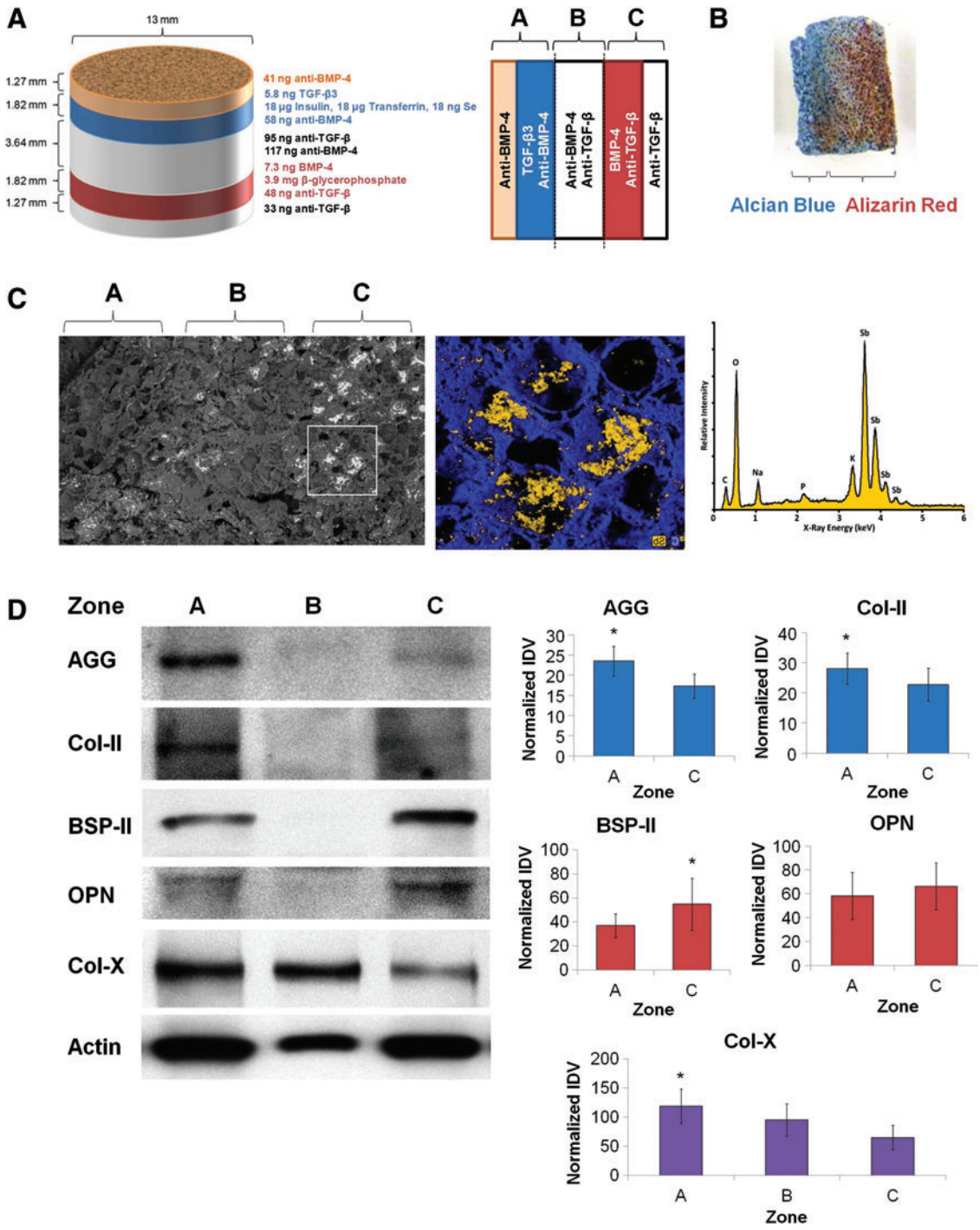

FIG. 6. Directed differentiation of MSCs into juxtaposed cartilage and bone using segregated morphogen fields. **(A)** Schematic of scaffold dimensions and contents (*left*) and orientation of scaffolds for subsequent analysis (*right*). **(B)** Representative photograph of a 1-mm-thick section from scaffolds after fixation and dual staining with Alcian Blue and Alizarin Red. **(C)** Scanning electron micrograph (*left*) and *inset* area (*middle*) showing localized electron-dense precipitates on the 1-mm-thick section from scaffolds. Energy-dispersive X-ray spectroscopic analysis identified mineralized precipitates to comprise antimonate (*right*). **(D)** Scaffolds were dissected into three zones, homogenized, and analyzed by western blotting for production of aggrecan (AGG), type II collagen (Col-II), bone sialoprotein II (BSP-II), osteopontin (OPN), and type X collagen (Col-X). β-Actin was used as a loading control. Representative western blots (*left*) and quantification of integrated band density (*right*) are shown ($n=5$). *Asterisks* indicate statistical significance at $p<0.05$. Color images available online at www.liebertpub.com/tea

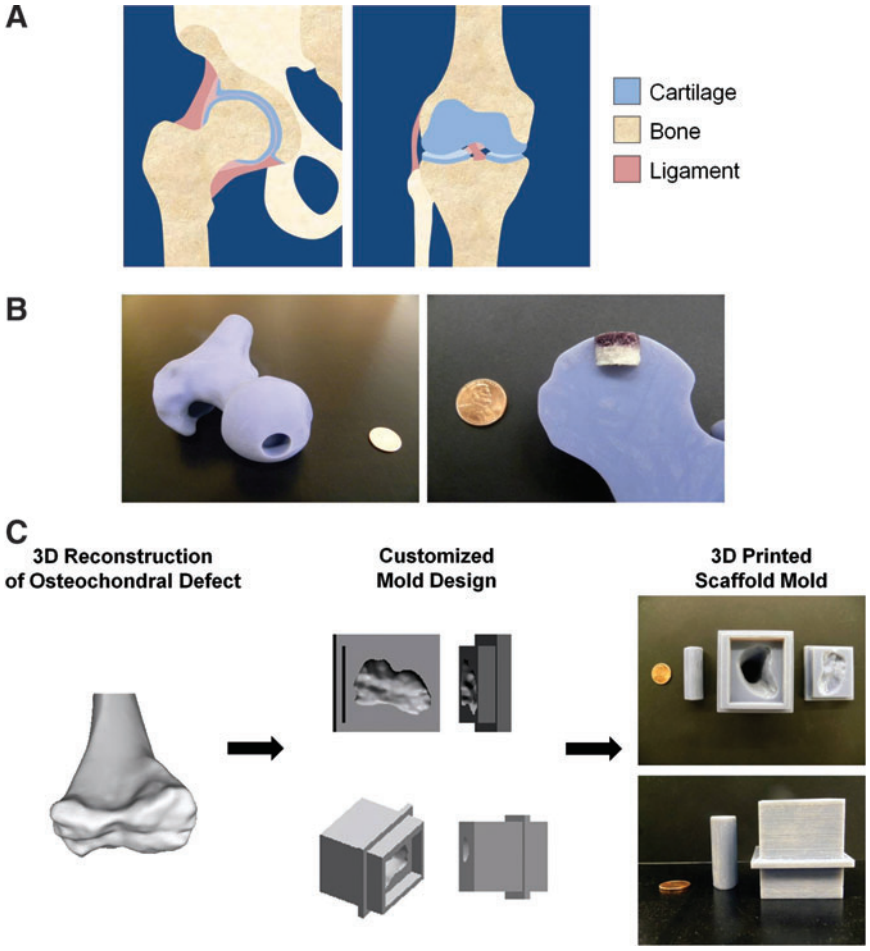

FIG. 7. Potential clinical applications for the multilayer scaffold system. **(A)** Anatomical drawings of juxtaposed bone and cartilage in the hip (coronal plane view, *left*) and knee (anterior view, *right*) joints. **(B)** Photographs of a cylindrical osteochondral defect in a model of a human femoral head (*left*) and insertion of the multilayer PLG scaffold in the defect model (*right*). **(C)** Proposed workflow of future clinical applications of these scaffold systems. A three-dimensional (3D) model of a human femur reconstructed from CT imaging (*left*) was used to design a customized scaffold mold in SolidWorks (*middle*), which was then 3D printed at 1:8 anatomical scale (*right*). Standard US pennies are shown for size comparison. Color images available online at www.liebertpub.com/tea

incorporation of cells within the scaffolds limits clinical utility by increasing the length of time between MSC harvest and implantation of the construct. In addition, maintaining the long-term differentiation of cells in the scaffold after dissociation can be a significant challenge. Ultimately, the use of multilayer PLG scaffolds, which present spatiotemporally regulated morphogen gradients to multipotent MSCs, not only allows for control of tissue geometry but may also abbreviate the time required to prepare bioengineered osteochondral constructs for implantation. Furthermore, incorporation of chemoattractant cues that facilitate recruitment of native host MSCs could potentially eliminate the need for exogenous cell transplantation.[7]

There are several limitations to the multilayer scaffold system developed in this study. First, tissues resulting from scaffolds seeded with MSCs were not mature enough after 21 days for histological analysis; therefore, our current endpoints are limited to molecular analyses of tissue production. Complete maturation of these constructs will require *in vivo* implantation. Ongoing experiments are utilizing the multilayer PLG scaffolds developed in this study for implantation in small and large animal osteochondral defect models. Second, while sharp gradients in growth factor activity were produced by incorporating neutralizing antibodies in selected scaffold layers, no such inhibitory agents exist for small-molecule cues such as β-glycerophosphate. Thus, although β-glycerophosphate was selectively incorporated in PLG microspheres used to fabricate the osteogenic layers of the scaffolds, diffusion of this small molecule throughout the system may have been responsible for the Alizarin Red staining noted in the middle layer. While diffusion of β-glycerophosphate, if it were appreciable, did not appear to interfere with chondrogenic differentiation, the utility of small molecules in the multilayer PLG scaffold system may be limited. Third, there appears to be reduced cellular activity within the central zone, despite loading identical quantities of total protein lysates, likely due to local cell death caused by hypoxia within the scaffold cores. We sought to engineer distinct layers of cartilage and bone, which were in contact with one another, to produce a construct with mechanical properties similar to native osteochondral tissue. In particular, we expected that the MSCs in zone B would spontaneously assume a mineralized bone-like phenotype over time (Fig. 2C). However, this phenomenon was likely compromised by necrosis of cells due to hypoxia caused by limited diffusion of oxygen within the scaffold core. Future iterations of this system could either reduce the thickness of the middle layer or alternatively incorporate proangiogenic factors to promote neovascularization from surrounding tissues into scaffold cores.[26] Fourth, differences in expression of chondrogenic and osteogenic matrix proteins were small across the scaffolds seeded with MSCs as the antibodies do not appear to completely neutralize all growth factors from opposing zones.

This study sought merely to produce significant gradients of morphogen concentration across the thickness of the scaffold and, in future studies, antibody concentrations may be increased to eliminate all morphogen activity in opposing zones of the scaffolds. This may ultimately allow differences in osteogenic and chondrogenic markers to become more pronounced between zones A and C. Finally, prominent detection of the type X collagen in zones A and B of the scaffolds indicates that some of the MSC-differentiated chondrocytes are undergoing hypertrophy and therefore mimicking endochondral ossification. Consistent with that process, the hypertrophic chondrocytes in this zone did not produce significant amounts of aggrecan or type II collagen. To regulate this process, the scaffold system could be modified in the future to incorporate parathyroid hormone-related protein, which allows chondrogenic differentiation, but prevents hypertrophic maturation,[27] within the chondrogenic scaffold zone.

This multilayer PLG scaffold system that can direct differentiation of juxtaposed hyaline cartilage and bone may be useful in clinical applications for orthopedic tissue reconstruction at the hip and knee joints (Fig. 7A). The current constructs could be used as cylindrical plugs to repair osteochondral defects that have been surgically revised (Fig. 7B). Moreover, we envision that this system could also be used to create constructs for the repair of more geometrically complex osteochondral defects. In this paradigm, the specifications for customized scaffold molds would be informed by CT imaging, and 3D printing could then be used to fabricate the customized molds, as exemplified by prototype scaffold molds for reconstruction of the human femoral condyle (Fig. 7C). In summary, this work presents a precision-engineered approach to the modeling and generation of morphogen fields within biomaterial-based scaffold systems for a wide range of regenerative applications.

Acknowledgments

The authors thank Will Yuen for his assistance with mathematical modeling, Jaeyun Kim for help with fabricating nanoparticles, Daniel Rifkin, NYUMC, for providing TGF-β (p3TP-luc) and BMP (C2C12BRE) luciferase reporter cell lines, and James Weaver for his assistance with SEM-EDS analysis. This work was funded by the NIH (R01 DE013033).

Disclosure Statement

No competing financial interests exist.

References

1. Martin, I., Miot, S., Barbero, A., Jakob, M., and Wendt, D. Osteochondral tissue engineering. *J Biomech* **40,** 750, 2006.
2. Alhadlaq, A., and Mao, J.J. Tissue-engineered osteochondral constructs in the shape of an articular condyle. *J Bone Joint Surg Am* **87,** 936, 2005.
3. Sharma, B., and Elisseeff, J.H. Engineering structurally organized cartilage and bone tissues. *Ann Biomed Eng* **32,** 148, 2004.
4. Alhadlaq, A., Elisseeff, J.H., Hong, L., Williams, C.G., Caplan, A.I., *et al.* Adult stem cell driven genesis of human-shaped articular condyle. *Ann Biomed Eng* **32,** 911, 2004.
5. Caplan, A.I. Embryonic development and the principles of tissue engineering. *Novartis Found Symp* **249,** 17, 2003.
6. Arany, P.R., and Mooney, D.J. At the edge of translation–materials to program cells for directed differentiation. *Oral Dis* **17,** 241, 2011.
7. Discher, D.E., Mooney, D.J., and Zandstra, P.W. Growth factors, matrices, and forces combine and control stem cells. *Science* **324,** 1673, 2009.
8. Lutolf, M.P., and Hubbell, J.A. Synthetic biomaterials as instructive extracellular microenvironments for morphogenesis in tissue engineering. *Nat Biotechnol* **23,** 47, 2005.
9. Yuen, W.W., Du, N.R., Chan, C.H., Silva, E.A., and Mooney, D.J. Mimicking nature by codelivery of stimulant and inhibitor to create temporally stable and spatially restricted angiogenic zones. *Proc Natl Acad Sci U S A* **107,** 17933, 2010.
10. Arany, P.R., Huang, G.X., Gadish, O., Feliz, J., Weaver, J.C., *et al.* Multi-lineage MSC differentiation via engineered morphogen fields. *J Dent Res* **93,** 1250, 2014.
11. Bouffi, C., Thomas, O., Bony, C., Giteau, A., Venier-Julienne, M.C., *et al.* The role of pharmacologically active microcarriers releasing TGF-β3 in cartilage formation *in vivo* by mesenchymal stem cells. *Biomaterials* **31,** 6485, 2010.
12. Puetzer, J.L., Petitte, J.N., and Loboa, E.J. Comparative review of growth factors for induction of three-dimensional chondrogenesis in human mesenchymal stem cells isolation from bone marrow and adipose tissue. *Tissue Eng Part B Rev* **16,** 435, 2010.
13. Vinardell, T., Buckley, C.T., Thorpe, S.D., and Kelly, D.J. Composition-function relations of cartilaginous tissues engineered from chondrocytes and mesenchymal stem cell isolated from bone marrow and infrapatellar fat pad. *J Tissue Eng Regen Med* **5,** 673, 2011.
14. Plánka, L., Starý, D., Hlučilová, J., Klíma, J., Křen, L., Nečas, A., *et al.* Differentiation protocol for hyaline-cartilage-producing mesenchymal stem cells. *Eur Musculoskelet Rev* **4,** 80, 2009.
15. de Gorter, D.J., van Dinther, M., Korchynskyi, O., and ten Dijke, P. Biphasic effects of transforming growth factor β on bone morphogenetic protein-induced osteoblast differentiation. *J Bone Miner Res* **26,** 1178, 2011.
16. Cordonnier, T., Langonné, A., Sohier, J., Layrolle, P., Rosset, P., *et al.* Consistent osteoblast differentiation of human mesenchymal stem cells with bone morphogenetic protein 4 and low serum. *Tissue Eng Part C Methods* **17,** 249, 2011.
17. Sammons, J., Ahmed, N., El-Sheemy, M., and Hassan, H.T. The role of BMP-6, IL-6, and BMP-4 in Mesenchymal stem cell-dependent bone development: effects on osteoblastic differentiation induced by parathyroid hormone and vitamin D_3. *Stem Cells Dev* **13,** 273, 2004.
18. Mooney, D.J., Baldwin, D.F., Suh, N.P., Vacanti, J.P., and Langer, R. Novel approach to fabricate porous sponges of poly(D,L-lactic-co-glycolic acid) without the use of organic solvents. *Biomaterials* **17,** 1417, 1996.
19. Harris, L.D., Kim, B.S., and Mooney, D.J. Open pore biodegradable matrices formed with gas foaming. *J Biomed Mater Res* **42,** 396, 1998.
20. Young, M.E., Carroad, P.A., and Bell, R.L. Estimation of diffusion coefficients of proteins. *Biotechnol Bioeng* **22,** 947, 1980.

21. Morell, A., Terry, W.D., and Waldman, T.A. Metabolic properties of IgG subclasses in man. *J Clin Invest* **49,** 673, 1970.
22. Paul, H., Reginato, A.J., and Schumacher, H.R. Alizarin red S staining as a screening test to detect calcium compounds in synovial fluid. *Arthritis Rheum* **26,** 191, 1983.
23. Whiteman, P. The quantitative measurement of Alcian Blue-glycosaminoglycan complexes. *Biochem J* **131,** 343, 1973.
24. Fernley, H.N., and Walker, P.G. Kinetic behavior of calf-intestinal alkaline phosphatase with 4-methylumbelliferyl phosphate. *Biochem J* **97,** 95, 1965.
25. Bauer, P.J. Affinity and stoichiometry of calcium binding by arsenazo III. *Anal Biochem* **110,** 61, 1981.
26. Kaigler, D., Wang, Z., Horger, K., Mooney, D.J., and Krebsbach, P.H. VEGF scaffolds enhance angiogenesis and bone regeneration in irradiated osseous defects. *J Bone Miner Res* **21,** 735, 2006.
27. Weiss, S., Hennig, T., Bock, R., Steck, E., and Richter, W. Impact of growth factors and PTHrP on early and late chondrogenic differentiation of human mesenchymal stem cells. *J Cell Physiol* **223,** 84, 2010.

Address correspondence to:
David J. Mooney, PhD
Harvard University School of Engineering and Applied Sciences
Pierce Hall Room 325
29 Oxford Street
Cambridge, MA 02138

E-mail: mooneyd@seas.harvard.edu

Received: February 24, 2015
Accepted: April 27, 2015
Online Publication Date: June 4, 2015